ACS APPLIED ELECTRONIC MATERIALS

Open Access
This article is licensed under CC-BY 4.0

An Aerosol-Assisted Chemical Vapor Deposition Route to Tin-Doped Gallium Oxide Thin Films with Optoelectronic Properties

Ruizhe Chen, Sanjayan Sathasivam, Joanna Borowiec, and Claire J Carmalt*

Cite This: https://doi.org/10.1021/acsaelm.4c00973 Read Online

ACCESS | Metrics & More | Article Recommendations | Supporting Information

ABSTRACT: Gallium oxide is a wide-bandgap compound semiconductor material renowned for its diverse applications spanning gas sensors, liquid crystal displays, transparent electrodes, and ultraviolet detectors. This paper details the aerosol assisted chemical vapor deposition synthesis of tin doped gallium oxide thin films using gallium acetylacetonate and monobutyltin trichloride dissolved in methanol. It was observed that Sn doping resulted in a reduction in the transmittance of Ga_2O_3 films within the visible spectrum, while preserving the wide bandgap characteristics of 4.8 eV. Furthermore, Hall effect testing revealed a substantial decrease in the resistivity of Sn-doped Ga_2O_3 films, reducing it from 4.2×10^6 Ω cm to 2×10^5 Ω cm for the 2.5 at. % Sn:Ga_2O_3 compared to the nominally undoped Ga_2O_3.

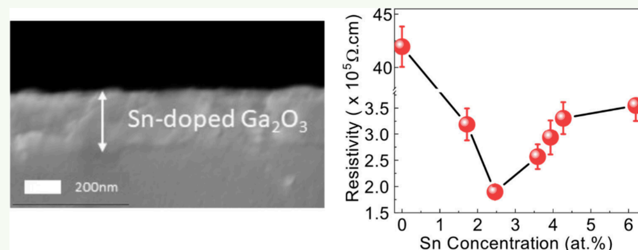

KEYWORDS: *Thin film, transparent conducting oxides (TCOs), gallium oxide (Ga_2O_3), chemical vapor deposition (CVD), dopants*

Downloaded via LONDON SOUTH BANK UNIV on August 21, 2024 at 16:20:36 (UTC).
See https://pubs.acs.org/sharingguidelines for options on how to legitimately share published articles.

■ INTRODUCTION

Gallium oxide (Ga_2O_3) is an emerging semiconductor material with application in power electronics, in photodetectors, and as transparent conducting oxides (TCOs).[1,2] Power devices founded upon β-Ga_2O_3 exhibit enhanced breakdown voltage and reduced on-resistance. Consequently, these devices result in diminished conduction loss and increased power conversion efficiency.[3−9] Moreover, devices made from Ga_2O_3 can operate at elevated temperatures, thus, mitigating the necessity for voluminous cooling mechanisms. The enhanced thermal performance stems from Ga_2O_3's capacity to endure augmented electric fields without undergoing breakdown, a capability that surpasses that of traditional materials such as silicon, SiC, and GaN.[3,10]

Ga_2O_3 also displays potential for power distribution systems in electric vehicle charging infrastructure or converters channeling energy from renewable sources such as wind turbines into the grid.[11−14] Furthermore, Ga_2O_3 emerges as a promising candidate for metal oxide semiconductor field effect transistors (MOSFETs), an electronic component ubiquitous in devices such as laptops and smartphones.[15,16] Ga_2O_3's viability extends to applications necessitating MOSFETs capable of operating at power levels surpassing the capabilities of traditional silicon-based devices.[1]

Ga_2O_3 thin films are also emerging as TCOs due to their ultrawide band gap of 4.8 eV and dopability with higher valence species such as Sn or Si to achieve enhanced conductivity.[17] TCOs are typically used in solar cells, flat panel displays, organic light-emitting diodes, specialized window coatings, transparent thin film transistors, and flexible electronic devices.[18−23] Ga_2O_3-based TCOs are particularly useful as electrodes for deep UV optoelectronic devices, such as lasers, LEDs, and detectors.[24]

The common methods for synthesizing Ga_2O_3 films include physical vapor deposition, chemical vapor deposition, solution deposition methods, pulsed laser deposition, and sputtering.[25−28] However, this study employs the aerosol-assisted chemical vapor deposition (AACVD) method to prepare Sn-doped Ga_2O_3 films. AACVD stands as a modification of the conventional CVD technique.[29−33] In this process, the precursor is initially dissolved in a solvent. Subsequently, this mixture of the precursor and solvent is transformed into a mist through an ultrasonic humidifier. The resulting mist is then introduced into the reactor via a carrier gas. In certain chemical reactions, the precursors undergo decomposition at elevated temperatures and the ensuing intermediates are simultaneously deposited onto the substrate.

In comparison to the aforementioned synthesis methods, AACVD offers advantages such as low cost, simple equipment and operation, a wide range of precursor compatibility, and convenient multimaterial doping. Basharat et al. have previously produced homogeneous and stable Ga_2O_3 films for gas sensing applications using AACVD.[34] Uno et al. have

Received: May 29, 2024
Revised: July 27, 2024
Accepted: July 29, 2024

© XXXX The Authors. Published by American Chemical Society

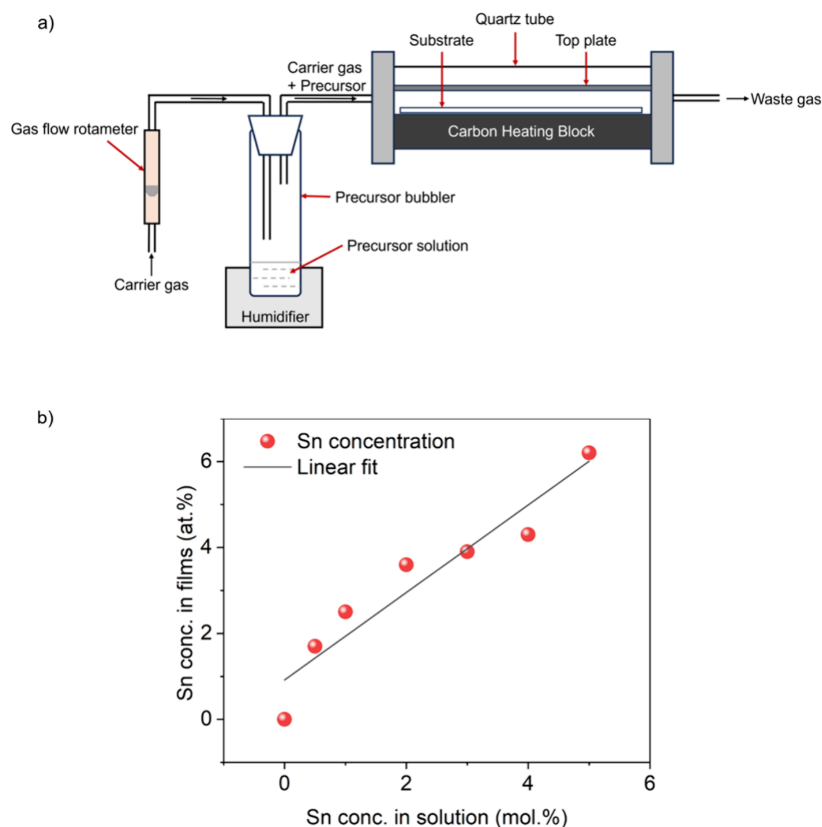

Figure 1. (a) Schematic diagram showing the process involved during aerosol assisted chemical vapor deposition (AACVD). (b) The linear relationship between the amount of MBTC in solution and the Sn concentration obtained in the doped Ga_2O_3 thin films grown via AACVD.

studied the growth mechanism of Ga_2O_3 on sapphire substrates using mist CVD. This study investigates the use of AACVD to deposit doped Ga_2O_3 films to enhance electronic conductivity.

EXPERIMENTAL SECTION

Film Synthesis. All precursor materials were procured from Aldrich and utilized without further purification. The AACVD depositions were conducted within a custom-designed cold-wall reactor.[35] In this setup, a quartz substrate measuring approximately 1 cm × 1 cm was placed on a glass substrate, while a graphite block, housing a Watlow cartridge heater regulated by a Pt−Rh cartridge heater, was positioned for controlled heating. To ensure laminar flow, a stainless-steel top plate was situated 0.8 cm above the substrate.

The Sn-doped Ga_2O_3 films were grown via an AACVD process, employing butyltin trichloride at varying concentrations (0, 0.5, 1, 2, 3, 4, and 5 mol %) and $Ga(acac)_3$ (0.3 g) dissolved in commercial dry methanol (20 mL, 788 mmol). The precursor solution was atomized using a Johnson Matthey Liquifog piezoelectric ultrasonic humidifier, with the precursor flow rate maintained at 0.5 L min^{-1} by nitrogen (BOC, 99.99%). The quartz substrate was maintained at a temperature of 450 °C throughout the deposition process.

Upon completion of deposition, the reactor was powered off and gradually cooled under a continuous flow of nitrogen until it reached 100 °C. At this juncture, the samples were carefully removed. Subsequently, the coated substrates were transferred to a tube furnace for heat treatment. The film and substrate were annealed in air at 1000 °C for a duration of 12 h.

Instrumental Conditions. X-ray diffraction (XRD) analysis was conducted using a PANalytical Empyrean system in grazing incidence mode with monochromated Cu Kα radiation. The incident beam angle was set at 0.5°, and the 2θ range of 5−80° was recorded with a step size of 0.05° at 1 s per step. Scanning electron microscopy (SEM) measurements were carried out by utilizing a JEOL JSM-6301F field emission SEM with a 5 keV accelerating voltage. To mitigate charging effects, the samples were coated with a layer of gold. X-ray photoelectron spectroscopy (XPS) was performed by using a Thermo Scientific Kα photoelectron spectrometer, which employed monochromatic Al Kα radiation. Higher resolution scans were acquired for the primary peaks of Sn(3d), Ga(3d), O(1s), and C(1s) with a pass energy of 50 eV. CasaXPS software was utilized for peak fitting, and binding energies were adjusted to adventitious carbon (284.8 eV) for charge correction. For resistivity (ρ) determination, Hall effect measurements were conducted by employing the van der Pauw method using a Ecopia HMS-3000 instrument.

RESULTS AND DISCUSSION

Nominally pure and Sn-doped Ga_2O_3 thin films were grown on quartz substrates from the AACVD reaction of gallium acetylacetonate ($Ga(acac)_3$), methanol, and monobutyltin trichloride (MBTC) at 450 °C (Figure 1a). The oxygen source for the films is thought to come from residual water in the methanol or the methanol itself and not directly from the breakdown of the oxygen containing acetylacetonate moiety of the organometallic precursor used for AACVD.[36] The concentration of MBTC was varied from 0, 0.5, 1, 2, 3, 4, and 5 mol % relative to $Ga(acac)_3$ to obtain Sn concentration of 0, 1.7, 2.5, 3.6, 3.9, 4.3, and 6.2 at. % in the films. This dopant concentration range was appropriate to study the impact of the Sn on the optoelectronic and material properties of the Ga_2O_3 thin films including the solubility limit of Sn in the Ga_2O_3 lattice. The atomic concentration in the film is largely increased with increasing concentration of the MBTC precursor in the AACVD, suggesting good compatibility with respect to the decomposition of both precursors during the CVD reaction (Figure 1b).

https://doi.org/10.1021/acsaelm.4c00973
ACS Appl. Electron. Mater. XXXX, XXX, XXX−XXX

Figure 2 displays the X-ray diffraction (XRD) patterns comprising of the calculated profiles for SnO_2 (cassiterite) and Ga_2O_3 (monoclinic), as well as patterns for Sn-doped Ga_2O_3 samples with Sn concentrations ranging from 0 to 6.2 at. % and the quartz substrate. The diffraction peak at approximately 22.4° is correlated to the SiO_2 substrate. For the 0−3.6 at. % doped samples, only peaks matching Ga_2O_3 were observed, indicating the successful formation of a solid solution. At the higher dopant concentrations of 3.9 to 6.2 at. %, a peak at 26.7° associated with the (110) plane of SnO_2 cassiterite becomes visible suggesting that the solubility limit of Sn in Ga_2O_3 has been reached and phase separation is taking place. The study by Guillermo et al. also addresses this issue, as the ionic radius of Sn^{4+} ions (0.69 Å) is larger (11.3%) than that of Ga^{3+} ions (0.62 Å), substitutional doping induces lattice distortion that can eventually lead to precipitation of a secondary phase from the solid solution.[37] In our CVD study, the solubility limit was visibly reached at 2.5 at. % Sn whereas other methods such as sputtering process and hydrothermal synthesis have reported Sn-doped Ga_2O_3 nanostructures with the solid solubility of around 1 atom % and 2.2 at. %, respectively.[27,38]

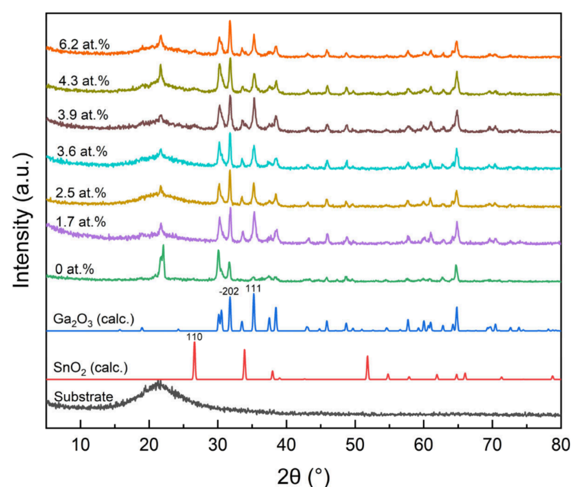

Figure 2. XRD patterns for the 0−6.2 at. % Sn-doped Ga_2O_3 films and quartz substrate. The calculated patterns for Ga_2O_3 and SnO_2 are also shown.

The incorporation of Sn as a dopant induces varied growth orientations in Ga_2O_3 films in comparison to the pristine Ga_2O_3 films, notably influencing the (−202) and (111) crystallographic directions.[39] Past studies have offered various explanations for the variation observed in diffraction peaks within X-ray diffraction (XRD) patterns with a predominant focus on the synthesis temperature of the films. Among the distinct structures of Ga_2O_3, β-Ga_2O_3 demonstrates stability at elevated temperatures, while α- and γ-Ga_2O_3 tend to crystallize more effectively at lower temperatures. Moreover, depending on the synthesis method employed and the substrate material chosen, there is a possibility of forming amorphous Ga_2O_3.[40−42] In contrast to the prevalent selection of silicon, β-Ga_2O_3, or sapphire as substrate materials in most investigations, the utilization of quartz substrates in this experiment facilitates Ga_2O_3 growth without predisposing it to a preferred tendency for epitaxial growth. A similar situation occurs in experiments where In_2O_3 is doped with different elements.[43] It is likely due to the change in surface energy and lattice parameter brought on by dopant atoms.

The full width at half-maximum (fwhm) of the XRD peaks decreased with increasing Sn concentration up to 2.5 at. %, indicating an increase in crystallinity and crystallite size. With further increase in dopant concentration, the fwhm increased again to values close to what was observed for the undoped Ga_2O_3 film (Table S1). Interestingly, the presence of the SnO_2 (110) peak becomes apparent as the Sn doping surpasses 2.5 at %. This shift signifies a transition from Sn-doped Ga_2O_3 to a composite of SnO_2/Ga_2O_3 at higher Sn concentrations.

The discernible alterations in the XRD diffraction peaks correspond to shifts in the film crystalline quality. In effect, marginal Sn doping contributes to the enhancement of Ga_2O_3 film crystalline quality. Yet, elevated Sn doping concentrations can lead to potential lattice disruption within the Ga_2O_3 films due to excessive Sn atom incorporation, potentially precipitating the formation of new phases (e.g., SnO_2). This occurrence subsequently diminishes the crystalline quality of the Sn-doped Ga_2O_3 films.[20]

Figure 3 depicts the transmission spectra of Sn-doped Ga_2O_3 films, delineating their response to varying Sn-doping concentrations. These samples exhibit a consistent average transmittance spanning 60% to 85% across both visible wavelength domains. Sn-doped Ga_2O_3 films show reduced transmittance in the visible spectrum compared with undoped

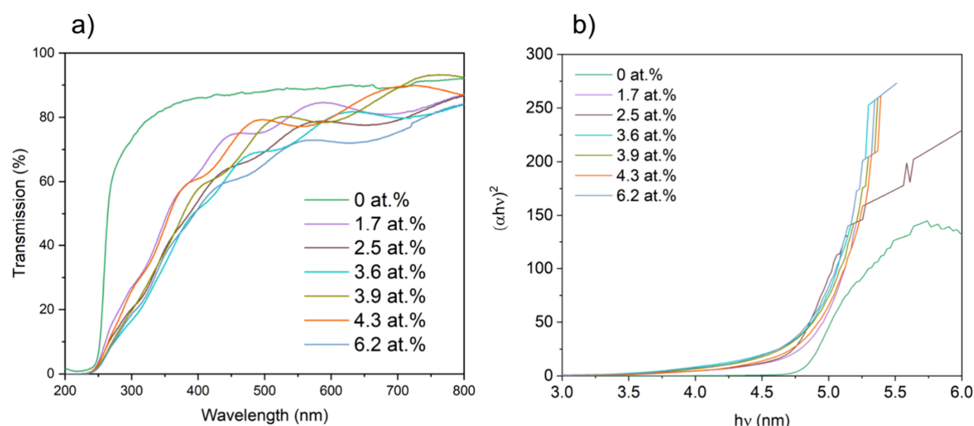

Figure 3. (a) Transmittance spectra of the undoped and Sn-doped Ga_2O_3 films grown on quartz substrates and (b) calculated Tauc plot indicating the direct band gap energies.

https://doi.org/10.1021/acsaelm.4c00973
ACS Appl. Electron. Mater. XXXX, XXX, XXX−XXX

films. Furthermore, an increase in the Sn doping content is correlated with an intensified light absorption propensity of the Ga_2O_3 films, particularly evident within the ultraviolet wavelength range (200−400 nm). When considering Ga_2O_3 films, the band gap (E_g) can be computed by utilizing the equation: $\alpha h\nu = A(h\nu - E_g)^{1/2}$. Here, α signifies the absorption coefficient, h stands for Planck's constant, ν represents the incident light frequency, and A denotes the material-specific constant.[44−46] For both the undoped and Sn doped Ga_2O_3 films, a band gap of 4.8 eV was observed.

Figure 4 illustrates the surface morphology of Ga_2O_3 films at varying Sn doping concentrations. An obvious trend emerges as the Sn doping concentration increases: the grain size becomes more uniform, resulting in a smoother and flatter film surface. Specifically, when the Sn doping concentration remains below 2.3 at. %, a coexistence of relatively larger grains, ranging from 150 to 250 nm in diameter, and finer particles was observed on the film surface. However, upon reaching a Sn doping concentration of 2.5 at%, the surface morphology of the Ga_2O_3 film showed a higher degree of uniformity, with grain sizes primarily concentrated within the 100−150 nm range. At higher doping concentrations, the SEM images reveal the presence of fine cracks. These cracks are most likely due to the annealing step applied to the films to obtain the monoclinic phase of Ga_2O_3 or the alteration of internal stress within the film due to changes in grain size. The alteration in surface morphology observed in the films could potentially be attributed to the annealing process, a phenomenon seen in previous research.[47] Upon deposition of Ga_2O_3 films onto sapphire substrates followed by annealing, grain-like structures emerged on the film surface, while internal grain boundaries were not discernible. These grain-like structures were identified to be associated with β-Ga_2O_3.

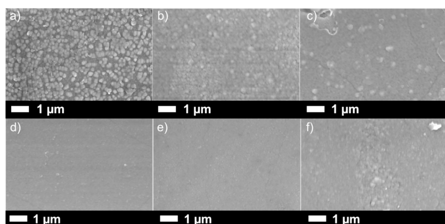

Figure 4. SEM images showing a faceted morphology for (a) 1.7 at%; (b) 2.5 at%; (c) 3.6 at%; (d) 3.9 at%; (e) 4.3 at%; (f) 6.2 at% Sn-doped Ga_2O_3 films annealed in air at 1000 °C for 12 h.

Concurrently, the cross-sectional analysis of the samples using SEM provides insights into the thickness of the Ga_2O_3 film deposited on the substrate (see ESI, Figure S1). As depicted in side-SEM results, the data suggest that the Sn doping concentration exerts minimal influence on the thickness of the Ga_2O_3 films, all of which fall within the range of 240−350 nm. Based on the side-view SEM results, it is evident that the doping of Sn induces a gradual granulation of the Ga_2O_3 microstructure, although obvious grain boundaries are not readily observed as seen in previous research.[47,48]

To investigate the composition of the Ga_2O_3 film, X-ray photoelectron spectroscopy (XPS) analysis was conducted, and the results are presented in Figure 5. Fitting of the surface Ga 3d and Sn 3d scans reveal Ga to be in the 3+ (Ga $3d_{5/3}$ centered at 20.5 eV) and Sn in 4+ (Sn $3d_{5/2}$ centered at 486.4 eV) oxidation states for all the films. For the C 1s core level, the primary peak is centered at 284.8 eV, corresponding to the C−C bond. Additionally, two secondary peaks are seen at 286.8 and 289.1 eV, signifying the presence of the C−O and C═C bonds, respectively, which is consistent with the findings in the reference literature.[49] The O 1s spectra were fit with three peaks. The principal component, situated at 530.9 eV, corresponds to the Ga−O bond, constituting the predominant component of the Ga_2O_3 thin film. Two minor peaks, at 530.2 and 532.5 eV, can be matched with literature values corresponding to Sn−O and C−O bonds, respectively.[50,51] There is also the possibility of the existence of other O^{2-} adsorbed species, such as O−H bonds.

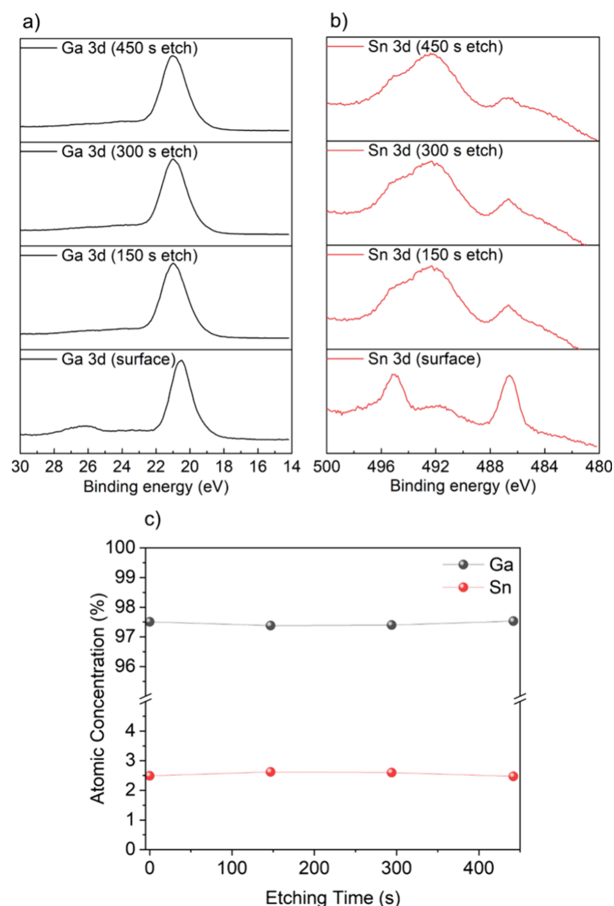

Figure 5. XPS of an 2.5 at% Sn-doped Ga_2O_3 film showing the (a) Ga 3d and (b) Sn 3d regions from the surface, 150, 300, and 450 s Ar etch to indicate the Sn dopant is present both on the surface and the bulk. (c) Trends in atomic concentration according to etching time.

Depth-resolved XPS analysis was also conducted on the doped films. As illustrated in Figure 5, a discernible disparity in the chemical environment was evident between the surface of the sample and the interior of the film. On the sample surface, a small peak appeared on the left side of the Ga 3d signal peak, which corresponds to the O 2s signal peak. However, this peak disappeared after etching, indicating the possible presence of adsorbates, or surface hydroxides on the thin film. These substances were absent from the interior of the sample. Similar results were also mentioned in the study by Ming−Ming et al.[26] The etching experiments also show a slightly higher Sn content in the interior of the thin film compared to that on its surface, possibly due to bulk segregation of the dopant. It should be noted that the differences in the Sn 3d peak shape seen at the surface and etched levels are due to preferential

sputtering effects that readily take place during etching of metal oxides under high vacuum.

Figure 6 presents the relationship between the Sn doping content and the film resistivity of Ga_2O_3 films. The resistivity

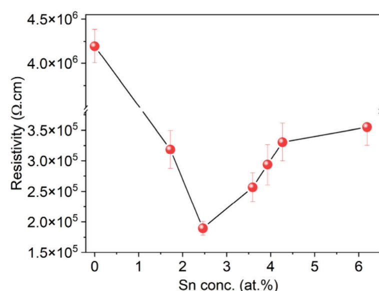

Figure 6. Electrical resistivity versus Sn atomic concentration for Sn-doped Ga_2O_3 films deposited on quartz via AACVD.

of the pristine Ga_2O_3 film measures approximately 4.2×10^6 Ω cm. Notably, a pronounced reduction in resistivity was observed following Sn doping, with the film exhibiting its lowest resistivity of 1.90×10^5 Ω·cm when the Sn concentration reached 2.5 at. %. The lowest resistivity was consistent with previous studies.[6] Overall, Ga_2O_3 crystals exhibit superior electrical performance compared to Ga_2O_3 thin films, which typically manifest resistivity values exceeding 10^{13} Ω cm. Maria Isabel Pintor-Monroy et al.[6] fabricated nanocrystalline thin films utilizing pulsed laser deposition (PLD) and molecular beam epitaxy (MBE) techniques, achieving a reduced resistivity of 2×10^5 Ω cm. Zhiwei Li et al.[52] employed the optical floating zone (OFZ) method to fabricate Ga_2O_3 thin films doped with Al elements, resulting in a resistivity of 1.5×10^{12} Ω cm. Wei Mi et al.[53] utilized the metal organic chemical vapor deposition (MOCVD) technique to synthesize Sn-doped Ga_2O_3 thin films, thereby decreasing the resistivity to 5.5×10^{12} Ω cm, reaching 5.4×10^7Ω cm with a 3 mol % Sn doping concentration.

Previous computational and analytical investigations have established that Sn doping enhances the concentration of free electrons without excessively diminishing their mobility within the material.[11,54−56] Concurrently, Sn doping may induce alterations in the crystal structure of the material such as lattice distortion or the introduction of crystal defects. Inspection of the XRD results reveal that Sn-doped Ga_2O_3 thin films exhibit an expansion in the unit cell volume, ranging from 0.9% to 1.5%, when compared to pure Ga_2O_3.

CONCLUSION

In summary, this study outlines the deposition process of Sn-doped Ga_2O_3 thin films on quartz substrates utilizing AACVD. With increasing dopant concentration a decrease in film resistivity was observed presumably due to increasing carrier density afforded by the Sn4+ substituting on Ga3+ sites in the Ga_2O_3 lattice. The lowest resistivity of 1.8×10^5 Ω cm was achieved for the 2.5 at. % Sn:Ga_2O_3 sample, this was more than an order of magnitude lower than that seen for the nominally undoped Ga_2O_3 film (4.2×10^6 Ω cm). Dopant concentrations beyond 2.5 at. % showed diminished electrical performance due to SnO_2 phase separation taking place. The ultrawide band gap of Ga_2O_3 was maintained at 4.8 eV even after doping.

ASSOCIATED CONTENT

Supporting Information

The Supporting Information is available free of charge at https://pubs.acs.org/doi/10.1021/acsaelm.4c00973.

Side on SEM, fwhm data, XPS spectra of C 1s and O 1s, Hall effect measurements (PDF)

AUTHOR INFORMATION

Corresponding Author

Claire J Carmalt − *Materials Chemistry Centre, Department of Chemistry, University College London, London WC1H 0AJ, U.K.*; orcid.org/0000-0003-1788-6971; Email: c.j.carmalt@ucl.ac.uk

Authors

Ruizhe Chen − *Materials Chemistry Centre, Department of Chemistry, University College London, London WC1H 0AJ, U.K.*; orcid.org/0009-0007-8595-8769

Sanjayan Sathasivam − *Materials Chemistry Centre, Department of Chemistry, University College London, London WC1H 0AJ, U.K.; School of Engineering, London South Bank University, London SE1 0AA, U.K.*; orcid.org/0000-0002-5206-9558

Joanna Borowiec − *Materials Chemistry Centre, Department of Chemistry, University College London, London WC1H 0AJ, U.K.*

Complete contact information is available at: https://pubs.acs.org/10.1021/acsaelm.4c00973

Notes

The authors declare no competing financial interest.

ACKNOWLEDGMENTS

Claire J. Carmalt and Joanna Borowiec thank the EPSRC for funding (EP/W010798/1). Sanjayan Sathasivam thanks the School of Engineering, London South Bank University for funding.

REFERENCES

(1) Green, A. J.; Speck, J.; Xing, G.; Moens, P.; Allerstam, F.; Gumaelius, K.; Neyer, T.; Arias-Purdue, A.; Mehrotra, V.; Kuramata, A.; et al. β-Gallium Oxide Power Electronics. *APL Mater.* **2022**, *10* (2), No. 029201.

(2) Yuan, Y.; Hao, W.; Mu, W.; Wang, Z.; Chen, X.; Liu, Q.; Xu, G.; Wang, C.; Zhou, H.; Zou, Y.; et al. Toward Emerging Gallium Oxide Semiconductors: A Roadmap. *Fundamental Research* **2021**, *1* (6), 697−716.

(3) Stepanov, S.; Nikolaev, V.; Bougrov, V.; Romanov, A. Gallium OXIDE: Properties and applica 498 a review. *Rev. Adv. Mater. Sci.* **2016**, *44*, 63−86.

(4) Higashiwaki, M.; Sasaki, K.; Kuramata, A.; Masui, T.; Yamakoshi, S. Development of Gallium Oxide Power Devices. *Physica Status Solidi (A) Applications and Materials Science* **2014**, *211* (1), 21−26.

(5) Singh, R.; Lenka, T. R.; Panda, D.; Velpula, R. T.; Jain, B.; Bui, H. Q. T.; Nguyen, H. P. T. Ga2O3 Based Heterostructure FETs (HFETs) for Microwave and Millimeter-Wave Applications. *Emerging Trends in Terahertz Engineering and System Technologies: Devices, Materials, Imaging, Data Acquisition and Processing* **2021**, 209−227.

(6) Quevedo-Lopez, M. A.; Pintor-Monroy, M. I.; Murillo-Borjas, B. L. Nanocrystalline and Polycrystalline β-Ga2O3 Thin Films for Deep Ultraviolet Detectors. *ACS Appl. Electron Mater.* **2020**, *2* (10), 3358−3365.

(7) Pearton, S. J.; Yang, J.; Cary, P. H.; Ren, F.; Kim, J.; Tadjer, M. J.; Mastro, M. A. A Review of Ga_2O_3Materials, Processing, and Devices. *Applied Physics Reviews* **2018**, *5* (1), 011301.

(8) Sheoran, H.; Kumar, V.; Singh, R. A Comprehensive Review on Recent Developments in Ohmic and Schottky Contacts on Ga_2O_3 for Device Applications. *ACS Applied Electronic Materials* **2022**, *4* (6), 2589−2628.

(9) Chen, X.; Ren, F.; Gu, S.; Ye, J. Review of Gallium-Oxide-Based Solar-Blind Ultraviolet Photodetectors. *Photonics Res.* **2019**, *7* (4), 381−415.

(10) Sasaki, K.; Kuramata, A.; Masui, T.; Víllora, E. G.; Shimamura, K.; Yamakoshi, S. Device-Quality β-Ga_2O_3 epitaxial Films Fabricated by Ozone Molecular Beam Epitaxy. *Applied Physics Express* **2012**, *5* (3), No. 035502.

(11) Litimein, F.; Rached, D.; Khenata, R.; Baltache, H. FPLAPW Study of the Structural, Electronic, and Optical Properties of Ga_2O_3: Monoclinic and Hexagonal Phases. *J. Alloys Compd.* **2009**, *488* (1), 148−156.

(12) Lee, C. T.; Chen, H. W.; Lee, H. Y. Metal-Oxide-Semiconductor Devices Using Ga_2O_3 Dielectrics on n-Type GaN. *Appl. Phys. Lett.* **2003**, *82* (24), 4304−4306.

(13) Baliga, B. J. Semiconductors for High-Voltage, Vertical Channel Field-Effect Transistors. *J. Appl. Phys.* **1982**, *53* (3), 1759−1764.

(14) Oshima, T.; Okuno, T.; Arai, N.; Suzuki, N.; Ohira, S.; Fujita, S. Vertical Solar-Blind Deep-Ultraviolet Schottky Photodetectors Based on β-Ga_2O_3 Substrates. *Applied Physics Express* **2008**, *1* (1), No. 011202.

(15) Zou, R.; Zhang, Z.; Liu, Q.; Hu, J.; Sang, L.; Liao, M.; Zhang, W. High Detectivity Solar-Blind High-Temperature Deep-Ultraviolet Photodetector Based on Multi-Layered (L00) Facet-Oriented β-Ga_2O_3 Nanobelts. *Small* **2014**, *10* (9), 1848−1856.

(16) Cora, I.; Mezzadri, F.; Boschi, F.; Bosi, M.; Čaplovičová, M.; Calestani, G.; Dódony, I.; Pécz, B.; Fornari, R. The Real Structure of ε-Ga_2O_3 and Its Relation to κ-Phase. *CrystEngComm* **2017**, *19* (11), 1509−1516.

(17) Zhang, J.; Willis, J.; Yang, Z.; Lian, X.; Chen, W.; Wang, L.-S.; Xu, X.; Lee, T.-L.; Chen, L.; Scanlon, D. O.; et al. Deep UV Transparent Conductive Oxide Thin Films Realized through Degenerately Doped Wide-Bandgap Gallium Oxide. *Cell Rep. Phys. Sci.* **2022**, *3* (3), No. 100801.

(18) Yoshioka, S.; Hayashi, H.; Kuwabara, A.; Oba, F.; Matsunaga, K.; Tanaka, I. Structures and Energetics of Ga_2O_3 Polymorphs. *J. Phys.: Condens. Matter* **2007**, *19* (34), No. 346211.

(19) Zinkevich, M.; Morales, F. M.; Nitsche, H.; Ahrens, M.; Rühle, M.; Aldinger, F. Microstructural and Thermodynamic Study of γ-Ga_2O_3. *Zeitschrift fuer Metallkunde/Materials Research and Advanced Techniques* **2004**, *95* (9), 756−762.

(20) Playford, H. Y.; Hannon, A. C.; Barney, E. R.; Walton, R. I. Structures of Uncharacterised Polymorphs of Gallium Oxide from Total Neutron Diffraction. *Chem.—Eur. J.* **2013**, *19* (8), 2803−2813.

(21) Kato, T.; Nishinaka, H.; Shimazoe, K.; Kanegae, K.; Yoshimoto, M. Demonstration of Bixbyite-Structured δ-Ga_2O_3 Thin Films Using β-Fe_2O_3 Buffer Layers by Mist Chemical Vapor Deposition. *ACS Appl. Electron Mater.* **2023**, *5* (3), 1715−1720.

(22) Zhao, D.; Sathasivam, S.; Li, J.; Carmalt, C. J. Transparent and Conductive Molybdenum-Doped ZnO Thin Films via Chemical Vapor Deposition. *ACS Appl. Electron Mater.* **2020**, *2* (1), 120−125.

(23) Jiamprasertboon, A.; Powell, M. J.; Dixon, S. C.; Quesada-Cabrera, R.; Alotaibi, A. M.; Lu, Y.; Zhuang, A.; Sathasivam, S.; Siritanon, T.; Parkin, I. P.; Carmalt, C. J. Photocatalytic and Electrically Conductive Transparent Cl-Doped ZnO Thin Films: Via Aerosol-Assisted Chemical Vapour Deposition. *J. Mater. Chem. A Mater.* **2018**, *6* (26), 12682−12692.

(24) Zhang, J.; Willis, J.; Yang, Z.; Lian, X.; Chen, W.; Wang, L.-S.; Xu, X.; Lee, T.-L.; Chen, L.; Scanlon, D. O.; Zhang, K. H.L. Deep UV Transparent Conductive Oxide Thin Films Realized through Degenerately Doped Wide-Bandgap Gallium Oxide. *Cell Rep. Phys. Sci.* **2022**, *3* (3), No. 100801.

(25) Mauze, A.; Zhang, Y.; Itoh, T.; Ahmadi, E.; Speck, J. S. Sn Doping of (010) β-Ga_2O_3 Films Grown by Plasma-Assisted Molecular Beam Epitaxy. *Appl. Phys. Lett.* **2020**, *117* (22), No. 222102.

(26) Fan, M. M.; Lu, Y. J.; Xu, K. L.; Cui, Y. X.; Cao, L.; Li, X. Y. Growth and Characterization of Sn-Doped β-Ga_2O_3 Thin Films by Chemical Vapor Deposition Using Solid Powder Precursors toward Solar-Blind Ultraviolet Photodetection. *Appl. Surf. Sci.* **2020**, *509*, No. 144867.

(27) Yoon, Y.; Kim, S.; Lee, I. G.; Cho, B. J.; Hwang, W. S. Electrical and Photocurrent Properties of a Polycrystalline Sn-Doped β-Ga_2O_3 Thin Film. *Mater. Sci. Semicond Process* **2021**, *121*, No. 105430.

(28) Mazeina, L.; Picard, Y. N.; Maximenko, S. I.; Perkins, F. K.; Glaser, E. R.; Twigg, M. E.; Freitas, J. A.; Prokes, S. M. Growth of Sn-Doped β-Ga_2O_3 Nanowires and Ga_2O_3-SnO_2 Heterostructures for Gas Sensing Applications. *Cryst. Growth Des* **2009**, *9* (10), 4471−4479.

(29) Mears, K. L.; Bhide, M. A.; Knapp, C. E.; Carmalt, C. J. Investigations into the Structure, Reactivity, and AACVD of Aluminium and Gallium Amidoenoate Complexes. *Dalton Transactions* **2021**, *51* (1), 156−167.

(30) Marchand, P.; Hassan, I. A.; Parkin, I. P.; Carmalt, C. J. Aerosol-Assisted Delivery of Precursors for Chemical Vapour Deposition: Expanding the Scope of CVD for Materials Fabrication. *Dalton Transactions* **2013**, *42* (26), 9406−9422.

(31) Powell, M. J.; Potter, D. B.; Wilson, R. L.; Darr, J. A.; Parkin, I. P.; Carmalt, C. J. Scaling Aerosol Assisted Chemical Vapour Deposition: Exploring the Relationship between Growth Rate and Film Properties. *Mater. Des* **2017**, *129*, 116−124.

(32) Chadwick, N.; Sathasivam, S.; Kafizas, A.; Bawaked, S. M.; Obaid, A. Y.; Al-Thabaiti, S.; Basahel, S. N.; Parkin, I. P.; Carmalt, C. J. Combinatorial Aerosol Assisted Chemical Vapour Deposition of a Photocatalytic Mixed SnO_2/TiO_2 Thin Film. *J. Mater. Chem. A Mater.* **2014**, *2* (14), 5108−5116.

(33) Sathasivam, S.; Arnepalli, R. R.; Kumar, B.; Singh, K. K.; Visser, R. J.; Blackman, C. S.; Carmalt, C. J. Solution Processing of GaAs Thin Films for Photovoltaic Applications. *Chem. Mater.* **2014**, *26* (15), 4419−4424.

(34) Basharat, S.; Carmalt, C. J.; Binions, R.; Palgrave, R.; Parkin, I. P. Gallium Oxide Thin Films from the AACVD of $[Ga(NMe_2)_3]_2$ and Donor Functionalized Alcohols. *Dalton Transactions* **2008**, No. 5, 591−595.

(35) Knapp, C. E.; Carmalt, C. J. Solution Based CVD of Main Group Materials. *Chem. Soc. Rev.* **2016**, *45* (4), 1036−1064.

(36) Uno, K.; Ohta, M.; Tanaka, I. Growth Mechanism of α-Ga_2O_3 on a Sapphire Substrate by Mist Chemical Vapor Deposition Using Acetylacetonated Gallium Source Solutions. *Appl. Phys. Lett.* **2020**, *117* (5), No. 052106.

(37) Gutierrez, G.; Sundin, E. M.; Nalam, P. G.; Zade, V.; Romero, R.; Nair, A. N.; Sreenivasan, S.; Das, D.; Li, C.; Ramana, C. V. Interfacial Phase Modulation-Induced Structural Distortion, Band Gap Reduction, and Nonlinear Optical Activity in Tin-Incorporated Ga_2O_3. *J. Phys. Chem. C* **2021**, *125* (37), 20468−20481.

(38) Ryou, H.; Yoo, T. H.; Yoon, Y.; Lee, I. G.; Shin, M.; Cho, J.; Cho, B. J.; Hwang, W. S. Hydrothermal Synthesis and Photocatalytic Property of Sn-Doped β-Ga_2O_3 Nanostructure. *ECS Journal of Solid State Science and Technology* **2020**, *9* (4), No. 045009.

(39) He, H.; Blanco, M. A.; Pandey, R. Electronic and Thermodynamic Properties β-Ga_2O_3. *Appl. Phys. Lett.* **2006**, *88* (26), 261904.

(40) Korotcenkov, G.; Brinzari, V.; Boris, I. (Cu, Fe, Co, or Ni)-Doped Tin Dioxide Films Deposited by Spray Pyrolysis: Doping Influence on Film Morphology. *J. Mater. Sci.* **2008**, *43* (8), 2761−2770.

(41) Zhuo, Y.; Chen, Z.; Tu, W.; Ma, X.; Pei, Y.; Wang, G. β-Ga 2 O 3 versus ε-Ga_2O_3: Control of the Crystal Phase Composition of Gallium Oxide Thin Film Prepared by Metal-Organic Chemical Vapor Deposition. *Appl. Surf. Sci.* **2017**, *420*, 802−807.

(42) Kumar, S. S.; Rubio, E. J.; Noor-A-Alam, M.; Martinez, G.; Manandhar, S.; Shutthanandan, V.; Thevuthasan, S.; Ramana, C. V.

Structure, Morphology, and Optical Properties of Amorphous and Nanocrystalline Gallium Oxide Thin Films. *J. Phys. Chem. C* **2013**, *117* (8), 4194−4200.
(43) Jansons, A. W.; Koskela, K. M.; Crockett, B. M.; Hutchison, J. E. Transition Metal-Doped Metal Oxide Nanocrystals: Efficient Substitutional Doping through a Continuous Growth Process. *Chem. Mater.* **2017**, *29* (19), 8167−8176.
(44) Roy, R.; Hill, V. G.; Osborn, E. F. Polymorphism of Ga2O3and the System Ga2O3−H2O. *J. Am. Chem. Soc.* **1952**, *74* (3), 719−722.
(45) Pugh, D.; Marchand, P.; Parkin, I. P.; Carmalt, C. J. Group 13 β-Ketoiminate Compounds: Gallium Hydride Derivatives as Molecular Precursors to Thin Films of Ga 2O 3. *Inorg. Chem.* **2012**, *51* (11), 6385−6395.
(46) Wang, C.; Zhang, J.; Xu, S.; Zhang, C.; Feng, Q.; Zhang, Y.; Ning, J.; Zhao, S.; Zhou, H.; Hao, Y. Progress in State-of-the-Art Technologies of Ga2O3devices. *J. Phys. D: Appl. Phys.* **2021**, *54* (24), No. 243001.
(47) KIM, H. Annealing Effects on the Properties of Ga2O3 Thin Films Grown on Sapphire by the Metal Organic Chemical Vapor Deposition. *Appl. Surf. Sci.* **2004**, *230* (1−4), 301−306.
(48) Kim, H. W.; Kim, N. H. Influence of Postdeposition Annealing on the Properties of Ga 2O3 Films on SiO2 Substrates. *J. Alloys Compd.* **2005**, *389* (1−2), 177−181.
(49) Higashiwaki, M.; Sasaki, K.; Murakami, H.; Kumagai, Y.; Koukitu, A.; Kuramata, A.; Masui, T.; Yamakoshi, S. Recent Progress in Ga2O3 Power Devices. *Semicond. Sci. Technol.* **2016**, *31* (3), No. 034001.
(50) Yuan, H.; Su, J.; Guo, R.; Tian, K.; Lin, Z.; Zhang, J.; Chang, J.; Hao, Y. Contact Barriers Modulation of Graphene/β-Ga2O3 Interface for High-Performance Ga2O3 Devices. *Appl. Surf. Sci.* **2020**, *527*, No. 146740.
(51) Guo, D.; Guo, Q.; Chen, Z.; Wu, Z.; Li, P.; Tang, W. Review of Ga2O3-Based Optoelectronic Devices. *Materials Today Physics* **2019**, *11*, No. 100157.
(52) Li, Z.; Chen, J.; Tang, H.; Zhu, Z.; Gu, M.; Xu, J.; Chen, L.; Ouyang, X.; Liu, B. Band Gap Engineering in β-Ga2O3for a High-Performance X-Ray Detector. *ACS Appl. Electron Mater.* **2021**, *3* (10), 4630−4639.
(53) Mi, W.; Li, Z.; Luan, C.; Xiao, H.; Zhao, C.; Ma, J. Transparent Conducting Tin-Doped Ga2O3 Films Deposited on MgAl2O4 (1 0 0) Substrates by MOCVD. *Ceram. Int.* **2015**, *41* (2), 2572−2575.
(54) Zacherle, T.; Schmidt, P. C.; Martin, M. Ab Initio Calculations on the Defect Structure of β-Ga 2O3. *Phys. Rev. B Condens Matter Mater. Phys.* **2013**, *87* (23), No. 235206.
(55) Hajnal, Z.; Miró, J.; Kiss, G.; Réti, F.; Deák, P.; Herndon, R. C.; Kuperberg, J. M. Role of Oxygen Vacancy Defect States in the N-Type Conduction of β-Ga2O3. *J. Appl. Phys.* **1999**, *86* (7), 3792−3796.
(56) Varley, J. B.; Schleife, A. Bethe-Salpeter Calculation of Optical-Absorption Spectra of In2O3 and Ga2O3. *Semicond. Sci. Technol.* **2015**, *30* (2), No. 024010.

https://doi.org/10.1021/acsaelm.4c00973
ACS Appl. Electron. Mater. XXXX, XXX, XXX−XXX